Modeling of the Dynamic Plasma Pinch in Plasma Focus Discharges Based in Von Karman Approximations

José H. González, Fabricio R. Brollo, and Alejandro Clausse

***Abstract*—Dynamic plasma pinches occur in a variety of devices, as Z-pinches and plasma focus. In this paper, a lumped parameter model of a dynamic plasma pinch produced in a plasma focus discharge is presented. The model is based in Von Karman approximations of the radial density and velocity profiles, which leads to the reduction to a system of ordinary differential equations describing the dynamic evolution of the pinch compression and expansion. The model was coupled with a fusion kernel to produce an estimate of the neutron yield per pulse. The calculations were tested against available data of the pressure–yield curve of seven experimental devices ranging from 1 to 250 kJ, showing excellent agreement, particularly regarding the curvature of the pressure–yield curve.**

***Index Terms*—Modeling, neutrons, pinch plasma, plasma focus, Von Karman integral method.**

I. Introduction

DENSE plasma pinching is a phenomenon occurring when an intense current is driven in a plasma column generating an azimuthal magnetic field that produces autoconfinement [1]. Plasma pinches are among the most efficient ways to achieve very high temperatures, and have wide applications in radiation production and pulse power [2]. In plasma focus devices, the plasma pinch is the result of the time evolution of the electrical discharge that travels along coaxial electrodes. A charged capacitor bank is connected to the closed end of the electrodes through a gaseous switch (spark gap), and the discharges normally start over the insulator separating the electrodes. Then, the plasma sheath takeoff axially and radially accelerated by the magnetic field generated by the current itself. After the current sheath runs over the open end of the central electrode, the plasma becomes rapidly compressed into a small column resulting in very hot and dense plasma pinch.

Several models were offered in the past to assist the design of plasma focus devices. Among the family of simple models, Mathuthu *et al.* [3] proposed a semiempirical model in which the sheath has both radial and axial variation during the run-down phase, and both the damped current and pinch length are allowed to vary with time. Later, Moreno *et al.* [4] derived a purely analytical model capable of explaining the relation of the neutron production with the gas-filling pressure and the geometrical parameters of the device, based in the thermonuclear component of the fusion reaction.

More sophisticated theories were applied to describe in detail the kinematics of the current sheath. Basque *et al.* [5] presented a 2-D snowplough including comparisons with experiments. Casanova *et al.* [6], [7] presented a finite-element approximation of plasma focus discharges, which reproduced very precisely the shape evolution of the sheath and the thermodynamics of the shock wave. Meanwhile, Stepniewski [8] proposed a numerical code based on the free-points method to solve a set of nonideal MHD equations including the kinetics of ionization.

On the other hand, lumped parameter models provide a useful intermediate approach in modeling. In general, this technique is valid whenever acceptable spatial profiles can be proposed for the main variables governing a given problem (Von Karman and Biot [9]). Lumped parameter models were applied with excellent results in plasma focus modeling, providing fast tools to assess the design and calibration of a wide range of energy devices. Lee [10] proposed a model based in the snow-plow approximation of the MHD equations, which was further extended to the simulation of different types of devices. Siahpoush *et al.* [11] and Goudarzi *et al.* [12] adapted Lee's model to the Filippov-type plasma focus geometry. Gonzalez *et al.* [13] presented a lumped parameter model of Mather-type plasma focus [14] based on plane pistons, which explained the experimental neutron production of numerous devices assuming a thermonuclear reaction mechanism in the pinch.

In this paper, an extension of Gonzalez *et al.* [13] model is presented, introducing a lumped parameter model of the pinch, based in the Von Karman integral method (Von Karman and Biot [9]). The model predictions are compared with available experimental data of different plasma focus devices, showing better agreement than previous works.

II. Description of the Model

Let us consider the pinch at the final stage of a plasma focus discharge (Fig. 1) as a hot plasma column containing an equal number of ions and electrons (i.e., $N_e = N_i$) in

Manuscript received March 20, 2009; revised May 12, 2009, June 24, 2009, July 6, 2009, and August 4, 2009. First published October 9, 2009; current version published November 11, 2009.

J. H. González and F. R. Brollo are with the National Atomic Energy Commission, CONICET, Buenos Aires, Argentina, and also with the Instituto Balseiro, 8400 Bariloche, Argentina (e-mail: pampa@cab.cnea.gov.ar; brollof@cab.cnea.gov.ar).

A. Clausse is with the National Atomic Energy Commission, CONICET, Buenos Aires, Argentina, and also with the PLADEMA, Universidad Nacional del Centro, 7000 Tandil, Argentina (e-mail: clausse@exa.unicen.edu.ar).

Digital Object Identifier 10.1109/TPS.2009.2030578

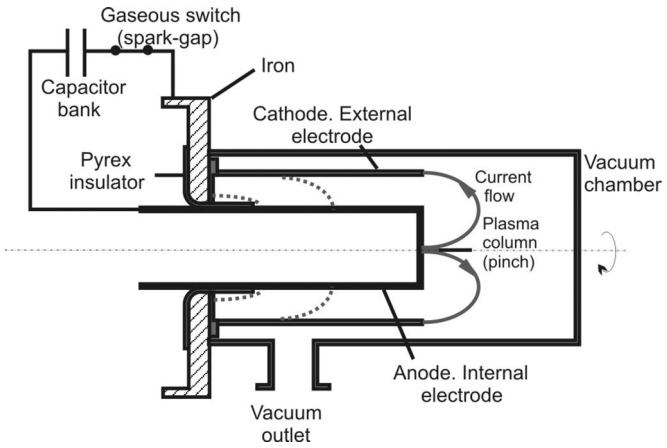

Fig. 1. Scheme of a plasma focus device.

thermal equilibrium (i.e., $T_e = T_i = T$). After the current sheet front reaches the axis, a shock wave reflection starts at $r = 0$ proceeding towards the pinch external face $(r = R)$, which, in turn, is moving toward the axis. The detailed modeling of this phenomenon would involve the solution of the compressible magnetohydrodynnamic equations. The alternative Von Karman method is to postulate a family of spatial profiles inside the pinch satisfying the expected boundary conditions at the center and the borders of the pinch. Following Von Karman approach, profiles of velocity and density will be proposed, and afterward used to integrate the conservation equations.

The velocity field inside the pinch should satisfy the following boundary conditions.

1) Zero radial velocity at the axis.
2) The pinch expands in the axial direction at sound velocity c_s.

Accordingly, the following profiles will be proposed for the radial v_r and axial v_z velocity components inside the pinch:

$$v_r(z,r,t) = \left(\frac{r}{R(t)}\right)^a v_R(t)$$

$$v_z(z,r,t) = \frac{2z}{h(t)} c_s(t) \tag{1}$$

where h is the pinch height, c_s is the average sound velocity at $z = \pm h/2$, v_R is the radial velocity at the pinch radius R (which is considered independent of z), and a is an effective constant parameter.

Analogously, the following density profile is assumed:

$$\rho(z,r,t) = \rho_o(t) - [\rho_o(t) - \rho_R(t)] \left(\frac{r}{R(t)}\right)^b \tag{2}$$

where ρ_o and ρ_R are the mass densities at the center and the outer boundary of the pinch, respectively, and b an effective constant parameter.

Assuming equipartition between ions and electrons energies, the pressure is related to the internal energy by

$$p(r,t) = 2(\gamma - 1)u(r,t) \tag{3}$$

where the ratio of specific heats γ is 5/3 for a totally ionized deuterium gas, and u is the energy per unit volume given by

$$u(r,t) = e(r,t) - \frac{1}{2}\rho(r,t)v^2(r,t) \tag{4}$$

and $e(r,t)$ is the total energy (internal plus kinetic) per unit volume. According to the assumed profiles, the pressure is a function of the time, the radial and axial position. However, regarding that the radial compression is much faster than the axial expansion, the profile will be averaged along the pinch length, which greatly simplifies the algebra. The radial pressure profile is then given by

$$p(r,t) = 2(\gamma - 1)\rho(r,t) \left\{ \frac{E_p}{M_p} - \frac{1}{4}\left[\frac{c_s^2}{3} + \left(\frac{r}{R}\right)^{2a} v_R^2\right]\right\} \tag{5}$$

where E_p and M_p are the total energy and mass of the pinch, which are related by $e(r,t) = (E_p/M_p)\rho(r,t)$.

According to Von Kárman method, the approximated profiles should satisfy globally the mass and momentum balances. The procedure is similar to the finite-element approach to numerically solve partial differential equations. In our case, (1), (2), and (5) should satisfy the mass and the radial-momentum balances

$$\frac{\partial \rho}{\partial t} + \frac{1}{r}\frac{\partial r\rho v_r}{\partial r} + \frac{\partial \rho v_z}{\partial z} = 0 \tag{6}$$

$$\frac{\partial(\rho v_r)}{\partial t} + \frac{1}{r}\frac{\partial(r\rho v_r^2)}{\partial r} = J_z B_\theta - \frac{\partial p}{\partial r} \tag{7}$$

where p is the pressure, and J_Z and B_θ are the axial current density and the azimuthal magnetic field, respectively, which assuming that the current is concentrated in the external face are given by

$$J_Z(r,t) = \frac{\delta(r-R)}{2\pi r} I(t)$$

$$B_\theta(r,t) = \frac{\mu_0}{4\pi}\frac{I(t)}{r}. \tag{8}$$

Integrating the continuity equation (6) over the pinch volume using the profiles given by (1) and (2), and regarding that the mass trapped in the pinch

$$M_p = \int_0^R \rho(r) h 2\pi r dr = h\pi R^2 \left(\frac{b\rho_o + 2\rho_R}{b+2}\right) \tag{9}$$

remains constant, the temporal evolution of ρ_o is determined by

$$\frac{d\rho_o}{dt} = 2\rho_R \frac{(a+b-2)}{b}\frac{v_R}{R} - \rho_o\left(\frac{2v_R}{R} + \frac{c_s}{h}\right). \tag{10}$$

Furthermore, evaluating (6) at $r = R$ gives

$$\frac{d\rho_R}{dt} = -\rho_R\left[(a+b)\frac{v_R}{R} + \frac{c_s}{h}\right]. \tag{11}$$

Analogously, integrating the radial momentum equation (7) over the pinch volume using the profiles given by (1), (2),

TABLE I
MAIN PARAMETERS OF THE EXPERIMENTS

Symbol	Parameter	Beg [19]	Moreno [4]	Kelly [23]	Rapp [25]	Nowikowski [24]	Peacock [16]	Maisonnier [20]
C	Capacity (μF)	32.7	10.5	46	3.36	21	96	1250
V	Initial voltage (kV)	11	30	16	85	36	25	20
E	Energy (kJ)	1.9	4.7	5.9	12.1	13.6	30	250
L_e	External inductance (nHy)	80	39	19	35	75	26	16
Z	Anode length (mm)	148	87	135	50	230	230	550
R_i	Anode radius (mm)	9	19	17	12.5	25	25	80
R_e	Cathode radius (mm)	50	36	50	42	50	50	120

and (4) gives

$$\frac{d}{dt}\left(\rho_{\text{eff}} v_R h R^2\right) = (a+2)hR\left(p_{\text{eff}} - p_M\right) \tag{12}$$

where ρ_{eff} and p_{eff} are effective density and counterpressure given by

$$\rho_{\text{eff}} = \frac{\rho_0 b + \rho_R(a+2)}{(a+2+b)} \tag{13}$$

$$\begin{aligned} p_{\text{eff}} = (\gamma-1)\rho_{\text{eff}} \Bigg\{ & \frac{\rho_0 b + \rho_R}{\rho_0 b + \rho_R(a+2)} \frac{a+2+b}{b+1} \frac{E_P}{M_P} \\ & - \Bigg[\frac{c_s^2}{6} \frac{\rho_0 b + \rho_R}{\rho_0 b + \rho_R(a+2)} \frac{a+2+b}{b+1} \\ & + \frac{\rho_0 b + \rho_R(2a+1)}{\rho_0 b + \rho_R(a+2)} \\ & \times \frac{a+2+b}{(2a+b+1)(2a+1)} \frac{v_R^2}{4a+2} \Bigg] \Bigg\} \end{aligned} \tag{14}$$

and p_M is the magnetic pressure

$$p_M = \frac{\mu_0 I^2}{8\pi R^2}. \tag{15}$$

It should also be mentioned that (9) is valid only for negative radial velocities. For positive radial velocities, after reaching the minimum radius, the radial expansion is constrained by the sound velocity.

Finally, the energy of the pinch E_p is calculated from the total energy balance of the entire system (pinch, current sheath, and external electric circuit), i.e.,

$$E = E_e + E_x + E_p \tag{16}$$

where E is the total energy of the system, which is invariant and therefore equals the initial capacitor energy. Strictly speaking, (16) requires the addition of an ionization energy consumption in the right-hand side. For deuterium, this amounts to roughly 16 eV per atom including the molecular dissociation energy. For PF devices of some kilojoule, this energy contribution is $\sim 10^{-10}$ J, which is negligible compared with the other terms. The electrical energy (capacitive and magnetic) E_e and the energy of the axial pinch E_x should be provided by the model of the circuit and the plasma gun. In what follows, the same model used in Gonzalez *et al.* [13] will be applied, and the interested reader is referred to it to avoid unnecessary diversions. In Appendix I, a brief description of the coupling equations between the external circuit and the run-down phase is provided.

Assuming a thermonuclear model, the neutron production is given by

$$\frac{dY}{dt} = \frac{1}{2} \int_{-h/2}^{h/2} dz \int_0^R n^2 \langle \sigma v \rangle 2\pi r dr \tag{17}$$

where n is the density of deuterons, and the average fusion cross section $\langle \sigma v \rangle$ depends on the temperature according to (Huba [15])

$$\langle \sigma v \rangle = 1.16810^{-12} T^{-2/3} e^{-187.6 T^{-1/3}} \tag{18}$$

where $\langle \sigma v \rangle$ is expressed in cubic meters per second, and the temperature T (in electronvolts) is calculated from the equation of state using the pressure and density profiles. Equation (17) is numerically calculated by means of the trapezium method.

III. MODEL VALIDATION

Equations (10)–(12) and (17) are combined to form a set of ordinary differential equations (see Appendix II) which are numerically solved using the FORTRAN LSODE subroutine package [17].

In order to validate the model, the numerical results were compared against the neutron data of seven experiments performed in different plasma focus devices available in the open literature (references found in Table I), with energies ranging from 1.9 to 250 kJ. Table I details the geometric and electrical parameters of the devices. All the experiments operated with deuterium and the dependence of the average neutron yield per pulse with the charging pressure was reported.

Table II details the values of the model parameters adjusted to fit the pressure–yield curve of each experiment, namely, the axial and radial shape parameters of the current sheath [13], and the pinch velocity and density profile exponents. Figs. 2–8) show the pressure dependence of the neutron yield together with corresponding numerical curve. In all cases, the compression factor was assumed $K = 4$, which is the typical value for planar supersonic shockwaves [18]. In the graphics, the results obtained with the previous model [13] is provided for comparison. It can be seen that the performance of the present

TABLE II
MODEL PARAMETERS OF EACH EXPERIMENT

Symbol	Parameter	Beg [19]	Moreno [4]	Kelly [23]	Rapp [25]	Nowikowski [24]	Peacock [16]	Maisonnier [20]
ξ_X	Axial shape parameter	0.08	0.50	0.50	0.35	0.80	0.80	0.9
ξ_R	Radial shape parameter	0.035	0.006	0.007	0.020	0.020	0.018	0.040
a	Velocity profile exponent	0.005	0.01	0.015	0.007	0.01	0.012	0.01
b	Density profile exponent	2.2	2.2	2.2	2.2	2.2	2.2	2.2

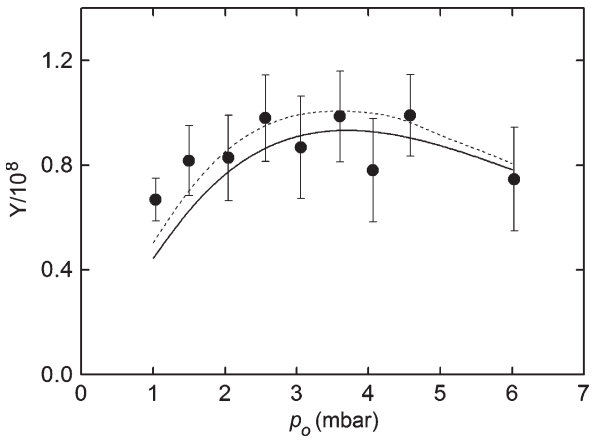

Fig. 2. Pressure–yield curve reported by Beg *et al.* [19]. (Points) Experimental data, (solid curve) present numerical calculation, and (dashed curve) results of the previous model.

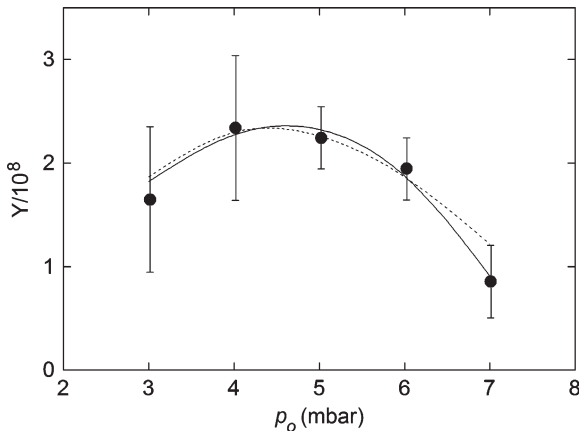

Fig. 3. Pressure–yield curve reported by Moreno *et al.* [4]. (Points) Experimental data, (solid curve) present numerical calculation, and (dashed curve) results of the previous model.

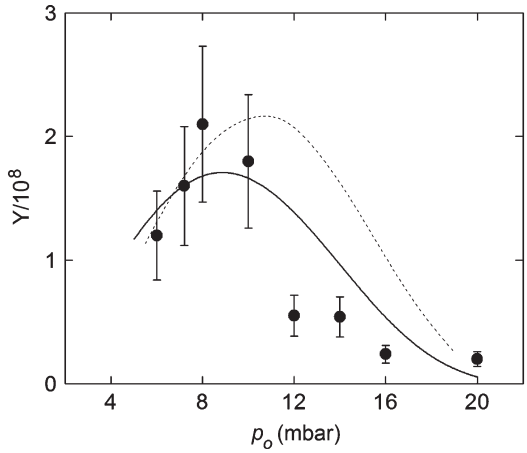

Fig. 4. Pressure–yield curve reported by Kelly [23]. (Points) Experimental data, (solid curve) present numerical calculation, and (dashed curve) results of the previous model.

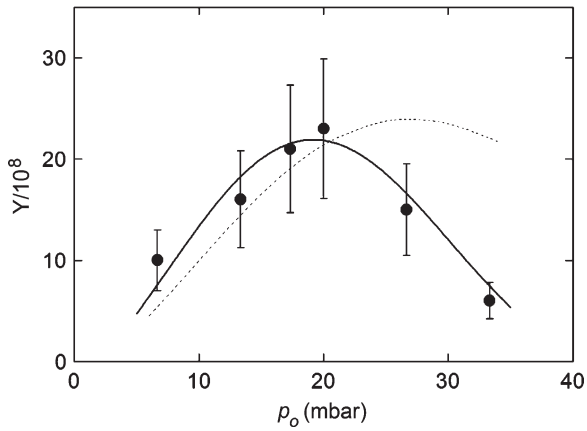

Fig. 5. Pressure–yield curve reported by Rapp [25]. (Points) Experimental data, (solid curve) present numerical calculation, and (dashed curve) results of the previous model.

model is much better, particularly regarding the curvature of the pressure–yield curve. This particular feature has being difficult to achieve in previous numerical models of plasma focus, either thermonuclear or beam-target based. It is worth noting that the model is able to correlate a wide range of energies and pressures.

IV. SENSITIVITY ANALYSIS

In order to analysis the sensitivity of the model results, the experiment reported by Beg *et al.* [19] was used as reference case. Figs. 9 and 10 show the sensitivity of the pressure–yield curve to 10% variations of the pinch velocity and density profiles parameters a and b. The corresponding sensitivity coefficients are

$$\frac{a}{Y}\frac{dY}{da} \cong 0.20$$
$$\frac{b}{Y}\frac{dY}{db} \cong 0.47. \tag{19}$$

V. IMPLICATIONS FOR CONTROLLED FUSION

Fig. 11 shows the contour map of the neutron yield dependence with the anode length (design parameter) and the filling pressure (operation parameter), corresponding to the

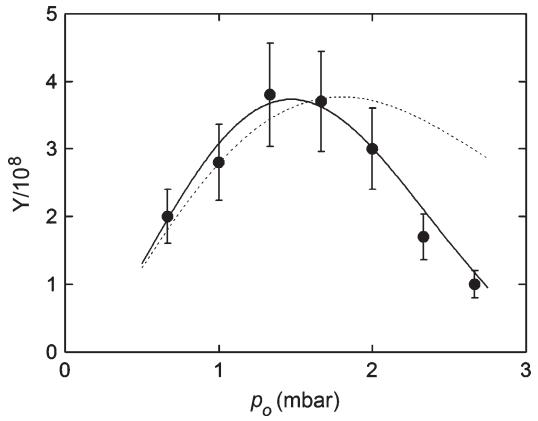

Fig. 6. Pressure–yield curve reported by Nowikowski [24]. (Points) Experimental data, (solid curve) present numerical calculation, and (dashed curve) results of the previous model.

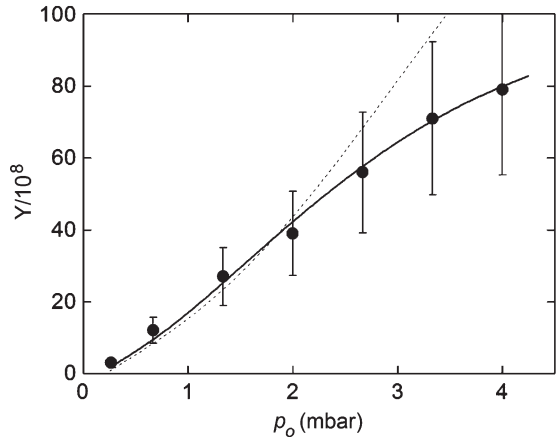

Fig. 7. Pressure–yield curve reported by Rapp [16]. (Points) Experimental data, (solid curve) present numerical calculation, and (dashed curve) results of the previous model.

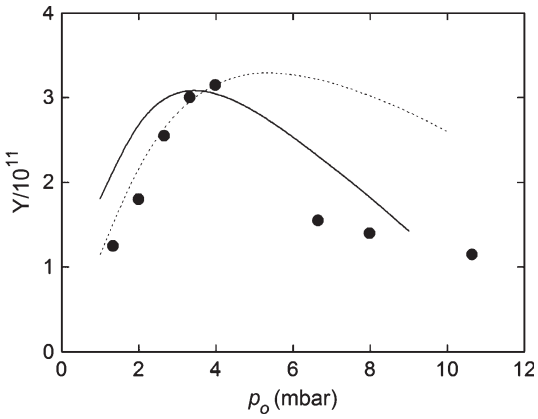

Fig. 8. Pressure–yield curve reported by Maisonnier *et al.* [20]. (Points) Experimental data, (solid curve) present numerical calculation, and (dashed curve) results of the previous model.

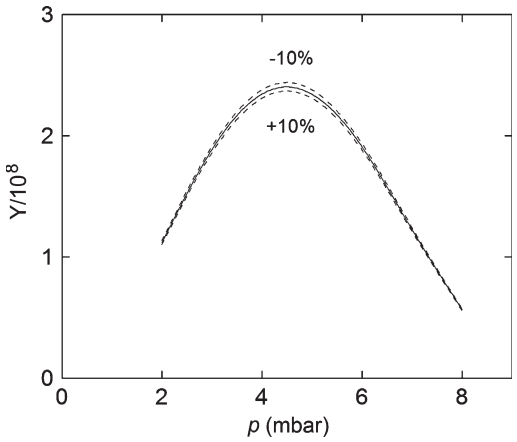

Fig. 9. Sensibility of the theoretical pressure–yield curve to variations of the velocity profile parameter a.

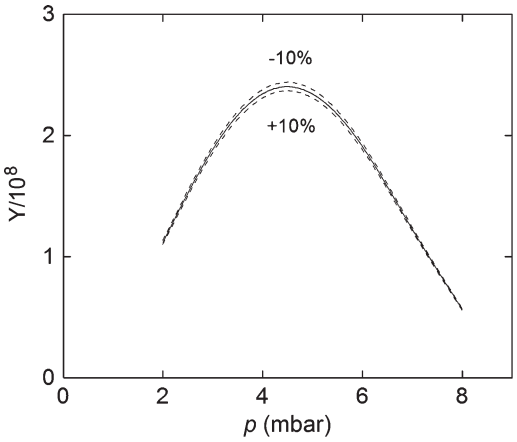

Fig. 10. Sensibility of the theoretical pressure–yield curve to variations of the density profile parameter b.

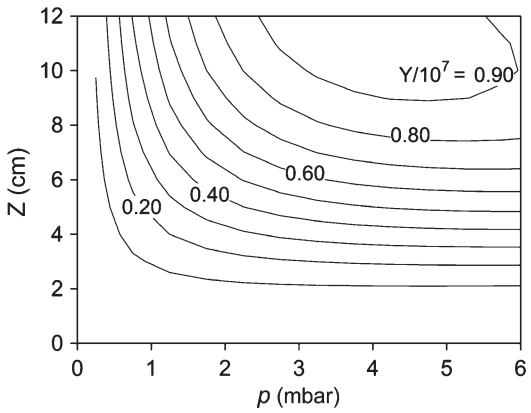

Fig. 11. Numerical calculation of the neutron-yield dependence with the charging pressure and the anode length (Beg *et al.* [19]).

experiment reported by Beg *et al.* [19]. It can be seen that there is an optimum combination of both parameters, which produce the maximum yield (keeping the charging voltage, 11 kV, and all other parameters constant). This optimum was actually measured in the referred experiment, and it is in agreement with the numerical calculation.

Using the present model, it is possible to estimate an upper limit for the amount of irreversible energy delivered to the current sheath and the pinch, by calculating the corresponding final internal and kinetic energy. The rest of the energy, in principle, can be recovered in the external capacitors (although a certain amount is lost by Joule effect and some energy is lost in the axial expansion). Nevertheless, the calculation of this upper limit for the unrecoverable energy per pulse can be used

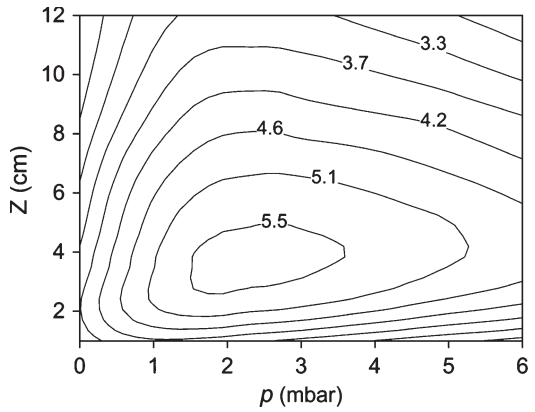

Fig. 12. Numerical calculation of the ratio between the fusion energy and the total energy delivered to the plasma (kinetic and internal) as function of the charging pressure and anode length (values are multiplied by 10^7), for the device reported in Beg *et al.* [19].

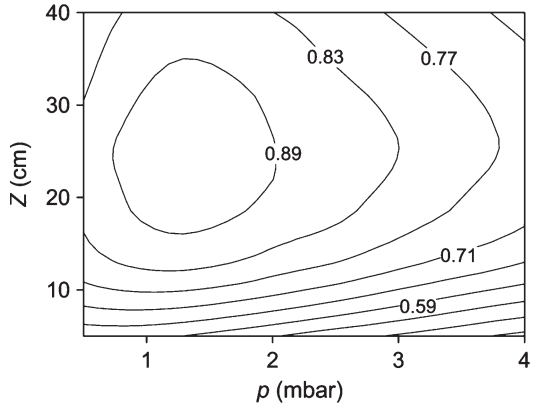

Fig. 13. Numerical calculation of the ratio between the fusion energy and the total energy delivered to the plasma (kinetic and internal) as function of the charging pressure and anode length (values are multiplied by 10^5), for the device reported in Maisonnier *et al.* [20].

to compare against the energy generated in the fusion reactions. Fig. 12 shows the contour map of the ratio between the fusion energy and the total energy delivered to the plasma (kinetic and internal) as a function of the charging pressure and anode length (keeping all other parameters constant), corresponding to the experiment reported by Beg *et al.* [19].

It is interesting to observe that there is a maximum energy ratio, but the optimum parameters here do not coincide with those corresponding to the maximum neutron yield. The maximum energy ratio is about 5.6×10^{-7}, which increases $\sim$250 times if a mixture of deuterium and tritium is used (i.e., 1.4×10^{-4}). The energy ratio can be increased by increasing the stored energy. Fig. 13 shows the contour map of the energy ratio for the 250-kJ device reported by Maisonnier *et al.* [20], showing a maximum value close to 10^{-5} (10^{-3} with deuterium–tritium).

VI. Conclusion

A lumped parameter model of a dense plasma pinch of Mather plasma focus discharges, based in Von Karman approximations of the inner velocity and density profiles, was presented. The model was coupled with a fusion kernel, which provides an estimate of the neutron yield per pulse. The calculations have been tested against available data of the pressure–yield curve of seven experimental devices ranging from 1 to 250 kJ, showing excellent agreement, particularly regarding the curvature of the pressure–yield curve. This particular feature has being difficult to achieve in previous numerical models of plasma focus.

Although it is true that the neutron yield anisotropies reported in several experiments suggest the existence of beam-driven fusion reactions in plasma foci, the results presented here show that the hypothesis of thermonuclear reactions as the main source of the neutrons seems to capture the average dependence of the pressure–yield curve at least in devices operating over 1 kJ. A possible interpretation of what happened with the beams inside the focus can be encountered by considering that the ion–electron and ion–ion equilibrium times go as $1/I$. Therefore, as the current increases, beam contributions to the fusion yield via beam-target interactions become heating contributions to the core pinch. Another possibility that should not be discarded is that neutron scatterings on the Hydrogen contained in the capacitors have lead to overestimations of the anisotropic components measured in the past. Nevertheless, it should be stressed that although the results presented in this paper does not preclude interpretations by other models, the model set out here does at least facilitate the raising of hypotheses and can be viewed as a measure of the quality of the devices, offering a simplified scenario for the evaluation and design of the dynamics and neutron production of plasma focus devices.

Appendix I

The current sheet during the run-down is represented by an annular piston moving forward in the axial direction. The mass and momentum equations of the plasma piston are

$$\frac{dM_X}{dt} = \xi \rho_g \pi \left(R_e^2 - R_i^2\right) V_X \tag{A1.1}$$

$$\frac{d(M_X V_X)}{dt} = \frac{1}{2} l I^2 \tag{A1.2}$$

where an axial sweep efficiency ξ is introduced to account for shape effects, V_X is the axial piston velocity, ρ_g the density of the stagnant gas ahead of the piston, and l is the linear inductance of the gun [21]

$$l = \frac{\mu_0}{2\pi} \ln\left(\frac{R_e}{R_i}\right). \tag{A1.3}$$

Assuming that the electric current flows at the backside of the sheet [22], the circuit equation is

$$\frac{d}{dt}\left\{[L_e + lX]\frac{dQ}{dt}\right\} + \frac{Q}{C} = 0 \tag{A1.4}$$

where X is the position of the piston backside, L_e is the inductance of the external circuit, Q the capacitor charge, and C the capacity.

On the sheet's arrival at the anode open end, the magnetic field accelerates the plasma toward the axis. Analogously, the

radial contraction is modeled by a planar cylinder whose length is determined by the axial piston [13].

The thickness of the axial piston δ_X is calculated regarding that the mass of the piston is

$$M_X = K\rho_g \pi \left(R_e^2 - R_i^2\right) \delta_X \tag{A1.5}$$

where K is the snowplow compression factor, and R_e and R_i are the external and internal electrodes radii, respectively [13].

APPENDIX II

The complete set of eight differential equations for the eight unknowns R, v_R, h, ρ_0, ρ_R, I, Q, and L, which describe the pinch dynamics, is detailed here. The auxiliary nondifferential equation for c_s is not numbered

$$\frac{dR}{dt} = \nu_R \tag{A2.1}$$

$$\frac{d}{dt}\left(\rho_{\text{eff}} v_R h R^2\right) = (a+2)hR(p_{\text{eff}} - p_M) \tag{A2.2}$$

$$\frac{d\rho_o}{dt} = 2\rho_R \frac{(a+b-2)}{b}\frac{v_R}{R} - \rho_o\left(\frac{2v_R}{R} + \frac{c_s}{h}\right) \tag{A2.3}$$

$$\frac{d\rho_R}{dt} = -\rho_R\left[(a+)\frac{\nu_R}{R} + \frac{c_s}{h}\right] \tag{A2.4}$$

$$\frac{dh}{dt} = c_s \tag{A2.5}$$

$$c_s^2 = c^2(\bar{r}, H) = \frac{2}{m_i}\gamma k T(\bar{r}, h)$$

$$= \frac{\frac{E_p}{M_P} - \frac{v_R^2}{2}\frac{2a\rho_R/(M_p/\pi h R^2)+b+2}{(2.a+b+2).(a+1)}}{\frac{1}{\gamma(\gamma-1)} + \frac{1}{2}}$$

$$\frac{d}{dt}(LI) = -\frac{Q}{C} \tag{A2.6}$$

$$\frac{dQ}{dt} = I \tag{A2.7}$$

$$\frac{dL}{dt} = \frac{\mu_0 c_s}{2\pi}\ln\left(\frac{R_e}{R}\right) - \frac{\mu_0 h}{2\pi}\frac{v_R}{R}. \tag{A2.8}$$

The variables ρ_{eff}, p_{eff}, and p_M are defined by (13)–(15) in Section II.

ACKNOWLEDGMENT

The authors would like to thank two anonymous reviewers that greatly help to improve the quality of this paper.

REFERENCES

[1] M. Liberman, J. De Groot, A. Toor, and R. Spielman, *Physics of High-Density Z-Pinch Plasmas*. New York: Springer-Verlag, 1999.

[2] C. Moreno, M. Venere, R. Barbuzza, M. Del Fresno, R. Ramos, H. Bruzzone, P. Florido, J. González, and A. Clausse, "Industrial applications of plasma focus radiation," *Braz. J. Phys.*, vol. 32, no. 1, pp. 20–25, Mar. 2002.

[3] M. Mathuthu, T. Zengeni, and A. Gholap, "The three-phase theory for plasma focus devices," *IEEE Trans. Plasma Sci.*, vol. 25, no. 6, pp. 1382–1388, Dec. 1997.

[4] C. Moreno, H. Bruzzone, J. Martínez, and A. Clausse, "Conceptual engineering of plasma focus thermonuclear pulsors," *IEEE Trans. Plasma Sci.*, vol. 28, no. 5, pp. 1735–1741, Oct. 2000.

[5] G. Basque, A. Jolas, and J. P. Watteau, "Comparison of two-dimensional snowplough with experiment," *Phys. Fluids*, vol. 11, no. 6, pp. 1384–1386, Jun. 1968.

[6] F. Casanova, C. Moreno, and A. Clausse, "Finite-elements numerical model of the current sheet movement and shaping in coaxial discharges," *Plasma Phys. Control. Fusion*, vol. 47, no. 8, pp. 1239–1250, Aug. 2005.

[7] F. Casanova, G. Correa, C. Moreno, and A. Clausse, "Experimental study and modeling of the plasma dynamics of magnetically driven shock waves in a coaxial tube," *Plasma Phys. Control. Fusion*, vol. 45, no. 12, pp. 1989–1999, Dec. 2003.

[8] W. Stepniewski, "MHD numerical modeling of the plasma focus phenomena," *Vacuum*, vol. 76, no. 1, pp. 51–55, Oct. 2004.

[9] T. Von Karman and M. Biot, *Mathematical Methods in Engineering: An Introduction to the Mathematical Treatment of Engineering Problems*. New York: McGraw-Hill, 1940.

[10] S. Lee, "A new theory for the fast compressional pinch," in *Proc. College Plasma Phys.*, Trieste, Italy, 1983, vol. 2, pp. 967–977.

[11] V. Siahpoush, M. Tafreshi, S. Sobhanian, and S. Khorram, "Adaptation of Sing Lee's model to the Filippov type plasma focus geometry," *Plasma Phys. Control. Fusion*, vol. 47, no. 7, pp. 1065–1075, Jul. 2005.

[12] S. Goudarzi, R. Amrollahi, and R. S. Moghaddam, "A model based on lumped parameters for Filippov-type plasma focus devices," *J. Fusion Energy*, vol. 27, no. 3, pp. 195–199, Sep. 2008.

[13] J. González, P. Florido, H. Bruzzone, and A. Clausse, "A lumped parameter model of plasma focus," *IEEE Trans. Plasma Sci.*, vol. 32, no. 3, pp. 1383–1391, Jun. 2004.

[14] J. Mather, "Dense plasma focus," in *Methods of Experimental Physics*, vol. 9B, H. Lovberg and H. Griem, Eds. New York: Academic, 1971, pp. 187–249.

[15] J. Huba, *NRL Plasma Formulary*. Washington, DC: Beam Phys. Branch, Plasma Phys. Div., Naval Res. Lab., 1998, p. 45.

[16] H. Rapp, "On the ground state of Ising chains with finite range interactions," *Phys. Lett. A*, vol. 43, no. 1, pp. 5–6, Feb. 1973.

[17] A. Hindmarsh, "Odepack, a sistematized collection of ODE solvers," in *Scientific Committing*, R. S. Stepleman, Ed. Amsterdam, The Netherlands: North Holland, 1983, pp. 55–64.

[18] J. D. Anderson, *Hypersonic and High-Temperature Gas Dynamics,* 2nd ed. Reston, VA: AIAA, 2006, p. 38.

[19] F. Beg, M. Zakaullah, M. Nisar, and G. Murtaza, "Role of the anode length in a Mather-type plasma focus," *Mod. Phys. Lett. B*, vol. 6, no. 10, pp. 593–597, 1992.

[20] C. Maisonnier, J. Rager, C. Gourlen, M. Galenti, and P. Morgan, "Preliminary results of the 1-MJ plasma focus experiment," in *Proc. IV Conf. Plasma Phys. Control. Nucl. Fusion Res.*, Berchtesgaden, Germany, 1976, vol. 3, pp. 447–453.

[21] S. Frish and A. Timoreva, *General Physics Course*, vol. II. Moscow, Russia: Mir, 1973, p. 481.

[22] G. Harnwell, *Principles of Electricity and Magnetism*, 2nd ed. New York: McGraw-Hill, 1949, p. 585.

[23] H. Kelly, "Régimen de operación de los equipos Plasma Focus desde el punto de vista de la optimización de la producción de reacciones de fusión," Ph.D. dissertation, Universidad de Buenos Aires, Buenos Aires, Argentina, 1983.

[24] J. Nowikowski, "Preliminary investigations of a non cylindrical Z pinch supplied from a 25 kJ current generator," *Nukleonika*, vol. 20, no. 12, pp. 1081–1090, 1974.

[25] H. Rapp, "Measurements referring to Plasma Focus Scaling laws," *Phys. Lett. A*, vol. 43, no. 5, pp. 420–422, Apr. 1973.

José H. González received the Nuclear Engineering and Ph.D. degrees from the Instituto Balseiro, Bariloche, Argentina, in 1994 and 2004, respectively.

He is a Professor of nuclear engineering with the Instituto Balseiro. Currently, he is also with the National Atomic Energy Commission, Buenos Aires, Argentina.

Dr. González is fellow of the National Science and Technology Council of Argentina.

Fabricio R. Brollo received the Mechanical Engineering degree from the Universidad Tecnológica Nacional, Buenos Aires, Argentina, in 1999 and the Nuclear Engineering degree from the Instituto Balseiro, Bariloche, Argentina, in 2005.

He is currently with the National Atomic Energy Commission, Buenos Aires, at the Research Reactor RA6. He is also an Instructor of nuclear engineering with the Instituto Balseiro.

Alejandro Clausse received the Nuclear Engineering and Ph.D. degrees from the Instituto Balseiro, Bariloche, Argentina, in 1981 and 1986, respectively.

From 1987 to 1990, he was a Visiting Scholar with Rensselaer Polytechnic Institute, Troy, New York. He is also a Professor of engineering with the Universidad Nacional del Centro, Tandil, Argentina, where he currently heads the PLADEMA Center of the Program of Dense Plasmas.

Dr. Clausse is a fellow of the National Council for Science and Technology of Argentina, and a member of the Institute of R&D, National Academy of Sciences, Buenos Aires.